




## Nonlinear, single-mode, two-dimensional Rayleigh-Taylor instability in ideal media

A. R. Piriz \* and J. J. López Cela 

*Instituto de Investigaciones Energéticas (INEI), E.T.S.I.I., and CYTEMA, Universidad de Castilla-La Mancha, 13071 Ciudad Real, Spain*

S. A. Piriz 

*Instituto de Investigaciones Energéticas (INEI), E.I.I.A., and CYTEMA, Universidad de Castilla-La Mancha, 45071 Toledo, Spain*

N. A. Tahir

*GSI Helmholtzzentrum für Schwerionenforschung Darmstadt, 64291 Darmstadt, Germany*



(Received 14 February 2024; accepted 1 August 2024; published 19 August 2024)

A model for the single mode, two-dimensional Rayleigh-Taylor instability in ideal, incompressible, immiscible, and inviscid fluids is developed as an extension of a previous linear model based on the Newton's second law [A. R. Piriz *et al.*, *Am. J. Phys.* **74**, 1095 (2006)]. It describes the transition from linear to nonlinear regimes and takes into account the mass of fluids participating in the motion during the instability evolution, including the laterally displaced mass. This latter feature naturally leads to the bubble and spike velocity saturation without requiring the usual drag term necessary in the well-known buoyancy-drag model (BDM). In addition, it also provides an explanation to the latter phase of bubble reacceleration without appealing to the vorticity generation due to the Kelvin-Helmholtz instability. The model is in perfect agreement with the BDM buoyancy-drag model, but, apart from extending its range of application, it solves many of its issues of concern and provides a more consistent physical picture.

DOI: [10.1103/PhysRevE.110.025101](https://doi.org/10.1103/PhysRevE.110.025101)

### I. INTRODUCTION

The Rayleigh-Taylor instability (RTI) is a ubiquitous phenomenon that occurs whenever a fluid of density  $\rho_1$  pushes and accelerates another fluid of density  $\rho_2 > \rho_1$  or, equivalently, when the latter lays on the top of the lighter fluid in a gravitational field [1–3]. This instability plays a central role in many natural processes ranging from astrophysics [4–7] to quotidian features like the falling of water when the container is inverted. It also determines the performance of many laboratory experiments on high-energy density physics [8–12] and serves as a tool for determining the mechanical properties of solids under high stress and strain conditions [13–20]. In addition, it is fundamental in the research on inertial confinement fusion (ICF) because it is the main factor that condition the minimum energy required for igniting a fuel capsule and obtaining high gain [21–26].

An extensive research by different methods, including theory, numerical simulations, and experiments, has been performed and detailed reviews can be found in Refs. [1–3]. However, many important aspects of the RTI physics are not yet well understood, especially in relation to the nonlinear regime that finally leads to the turbulent mixing of both media. This is true even for the simplest situation of a planar interface separating two semi-infinite ideal fluids submitted to a single mode perturbation in a uniform gravitational field. Such a situation has been widely studied by means the so-called

buoyancy-drag model (BDM), which yields phenomenological equations of motion for the spike and bubble evolutions and has been constructed to fit the results of experiments and numerical simulations [2,27–33]:

$$\begin{aligned} & \{(1 + C_a e^{-C_e k \xi_s}) \rho_2 + (C_a + e^{-C_e k \xi_s}) \rho_1\} \ddot{\xi}_s \\ & = (1 - e^{-C_e k \xi_s}) (\rho_2 - \rho_1) g(t) - C_d \rho_1 k \dot{\xi}_s^2, \end{aligned} \quad (1)$$

$$\begin{aligned} & \{(1 + C_a e^{-C_e k \xi_b}) \rho_1 + (C_a + e^{-C_e k \xi_b}) \rho_2\} \ddot{\xi}_b \\ & = (1 - e^{-C_e k \xi_b}) (\rho_2 - \rho_1) g(t) - C_d \rho_2 k \dot{\xi}_b^2, \end{aligned} \quad (2)$$

where, for the two-dimensional (2D) problem, it is  $C_a = 2$  and  $C_d = C_e = 3$  are constant parameters chosen to fit the results of experiments and simulations,  $g(t)$  is a uniform gravity acceleration,  $\xi_s$  and  $\xi_b$  are, respectively, the instantaneous amplitudes of the spike and the bubble, and  $k = 2\pi/\lambda$  is the perturbation wave number ( $\lambda$  is the perturbation wavelength).

Although the apparent simplicity of these equations, they actually masks several unsolved issues. As noticed by Dimonte [29], the inertia is uncertain because the total displaced masses of the fluid being penetrated by the spike and the bubble, respectively, are not taken into account or, at most, it is accounted by introducing an *ad hoc* constant parameter.

In addition, it has to include a drag force term in order to account for the saturation of the bubble velocity, for the case of Atwood number  $A_T = 1$  [ $A_T = (\rho_2 - \rho_1)/(\rho_2 + \rho_1)$ ], and of the bubble and spike velocities when  $A_T < 1$  [29,34]. Such a drag force should have origin in the viscosity of the

\*Contact author: roberto.piriz@uclm.es

involved fluids. However, velocity saturation is found to occur in inviscid potential models and numerical simulations [34,35], and viscosity should not be significant in most of ICF applications where saturation is still observed [24,36]. On the other hand, the effect of viscosity should rather be the inhibition or limitation of the reacceleration process taking place at late evolution times, which are not described by the BDM [37]. Besides, assuming that in the present case the drag force can be assimilated to the drag undergone by a solid body moving into a fluid [29], the drag coefficient  $C_d$  would hardly be a constant, but dependent of the Reynolds number in a manner that, in general, should be determined experimentally.

Furthermore, the reacceleration process, first observed in numerical simulations by Ramaprabhu *et al.* [38] and then confirmed by experiments by Wilkinson and Jacobs [39] arising when the bubble amplitude is  $\xi_b \approx \lambda$ , is commonly explained on the basis of the correlation with the onset of the Kelvin-Helmholtz instability (KHI) observed in the experiment and numerical simulations when  $A_T < 1$ . Namely, the argument is that the vortices generated by the KHI around the spike surface when it penetrates into the lighter fluid, propagate towards the bubble tip thus causing its reacceleration [37,40,41]. Such observed correlation, however, in any manner implies the existence of a causal relationship. In this regard, the argument resembles the one exposed by Aristoteles to explain the flight of an arrow [42]: “Although well clear of the archer’s bow, the arrow continues to move because the air which is parted at its forward tip circles ‘round behind, filling the void left by the advancing tail’; it thus impinges upon the after part of the arrowshaft, pressing it forward so as to continue its flight.”

As is well known, the argument inverts the causal relation between the motion of the arrow penetrating into the air, and the vortices generation due to the shear driven by such a motion, and leads to the paradoxical result that the air push the arrow instead to slow down it.

This argument is neither well supported by the evidence from numerical simulations in the RTI problem, which show that with sufficient resolution, bubble reacceleration would also happens for  $A_T = 1$  ( $\rho_1 = 0$ ) provided that the Reynolds numbers goes to infinite (inviscid limit), when no vortices could be generated by KHI. Moreover, Wilkinson and Jacobs [39] also noticed that, quite surprisingly, at low Atwood numbers, no reacceleration was observed in the experiments by Waddel *et al.* [43] although “the obvious and pronounced occurrence of vortices,” which once again seems to contradict a causal relation between the vorticity migration from the spike to the bubble and the bubble reacceleration.

The above discussed features put in evidence the necessity of a more consistent physical picture. For this, in this work we propose a new model based also in the Newton’s second law that uses and extends a previous model for the linear phase of RTI [44] and aims at solving the above mentioned issues. The model is presented in Sec. II, starting with a brief review of the linear model in Sec. II A.

Dimensional analysis and geometrical arguments are discussed in Sec. II B, and the generalization of the linear model to the nonlinear regime is presented in Sec. II C. Then, we analyze the asymptotic behavior of the solutions in Sec. II D,

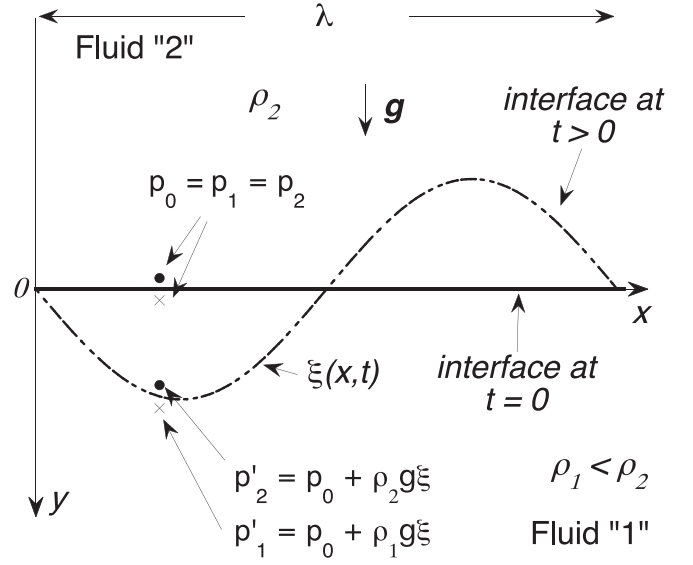


FIG. 1. Schematic of the early linear evolution of a perturbed interface between two fluids.

and we also compare the present model with the BDM results in Sec. II E.

In Sec. III, we extend the model for describing the reacceleration process, and in Sec. IV we present some comparisons of the model with 2D numerical simulations. Final discussion and remarks are given in Sec. V.

## II. THE PHYSICAL MODEL

### A. Review of the linear model

We start with a brief review of the linear model of Ref. [44], which basic features are summarized in Fig. 1. The model considers a situation in which at  $t = 0$  we have a fluid of density  $\rho_2$  on the top of a lighter fluid of density  $\rho_1 < \rho_2$  in a uniform gravitational field with gravity acceleration  $g = g(t)$ , which, in general, can be a function of the time  $t$ . Fluids are inviscid, incompressible, and immiscible.

If the interface is initially perfectly planar and in equilibrium, then the pressure on both sides of it will be the same:  $p_1 = p_2 \equiv p_0$ . When a perturbation  $\xi(x)$  is introduced at the interface, so that any fluid particle at  $y = 0$  is translated to  $y = \xi(x) > 0$ , the hydrostatic pressure on the new position of the interface changes in such a manner that it increases more on the side of the denser fluid than on the side of the lighter one. Therefore, the pressures on the interface new position become

$$p'_1 = p_0 + \rho_1 g \xi \quad p'_2 = p_0 + \rho_2 g \xi. \quad (3)$$

Then, a pressure difference  $\Delta p' = p'_2 - p'_1 = (\rho_2 - \rho_1)g\xi$  arises on the interface, which tends to further deform it, so driving the motion of the interface according to the Newton’s second law:

$$\frac{d(m\dot{\xi})}{dt} = (\rho_2 - \rho_1)g\xi, \quad (4)$$

where  $m$  is the total mass per unit area of both fluids that is participating in the motion due to the perturbation evolution. In

the linear regime ( $k\xi \ll 1$ ), the only significant characteristic length of the problem is  $k^{-1}$  and, therefore, the total effective mass (per unit area) involved in the motion is the one placed within a distance of the order of  $k^{-1}$  from the interface:

$$m = m_1 + m_2 = \frac{\rho_1}{k} + \frac{\rho_2}{k}. \quad (5)$$

Introducing this expression into Eq. (4), we get:

$$\ddot{\xi} = A_T k g \xi, \quad (6)$$

which, as is well known, correctly describes the evolution of the peaks and valleys in the linear regime provided that the condition  $k\xi \ll 1$  is satisfied. Notice that such a condition is only necessary for evaluating the amount of displaced mass of the fluids during the motion of the interface. But the buoyancy force  $F_B$  (per unit area) is determined by the hydrostatic pressure difference and it is always the force driving the instability at any time and independently of the magnitude of the perturbation amplitude:

$$F_B = (\rho_2 - \rho_1)g\xi. \quad (7)$$

Differently, the mass involved in the motion will change when the condition  $k\xi \ll 1$  breaks, and the new characteristic length  $\xi$  is introduced into problem and becomes also relevant.

### B. Dimensional analysis

When the two lengths of the problem,  $k^{-1}$  and  $\xi$ , become relevant, the characteristic distance  $l$  from the interface that determines the mass participating in the motion, will be a function of both of them:  $l = l(k, \xi)$ . Dimensional analysis indicates that this functional relationship can be expressed in dimensionless form as follows:

$$\phi = \phi(\Pi) \quad \Pi = k\xi, \quad (8)$$

which leads to two possible characteristic lengths:

$$kl_s = \phi(k\xi) \quad \frac{l_b}{\xi} = \phi(k\xi), \quad (9)$$

where  $\xi$  can be either the amplitude of the spike or of the bubble.

In the linear phase, when  $k\xi \ll 1$ , the complete similarity hypothesis demands that  $\phi \rightarrow \text{const}$ , and only  $l_1 \sim k^{-1}$  remains significant. When  $k\xi$  is not negligible, the hypothesis of incomplete similarity [45] yields the following expressions:

$$kl_s = C_1(k\xi)^\alpha \quad \frac{l_b}{\xi} = C_2(k\xi)^\alpha. \quad (10)$$

As it is well known, the power  $\alpha$  cannot be determined by dimensional analysis and it requires to resort to other means. As we will see by using geometrical arguments, it must be  $\alpha = 1$ , so that:

$$l_s = C_1 \xi \quad l_b = C_2 k \xi^2, \quad (11)$$

where  $C_{1,2}$  are constants to be determined by other methods. The existence of two possible characteristic lengths determining the mass put in motion by the instability once the system has overcome the linear regime, can be associated to the asymmetric growth of peaks and valleys that gives place to the rise of spikes and bubbles, respectively. Therefore, in

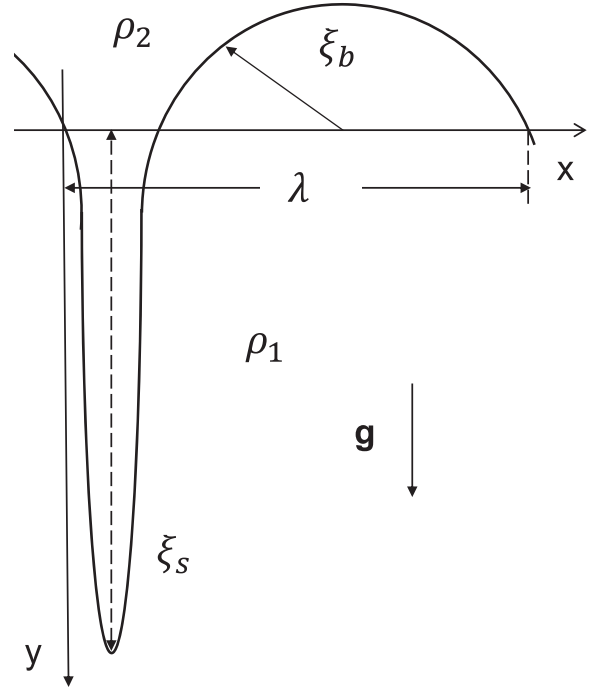


FIG. 2. Schematic of the early nonlinear evolution of a perturbed interface between two fluids.

Eq. (11) and hereafter we distinguish the respective amplitudes of the spike and the bubble with the subindexes “s” and “b.” In particular, it is worth to notice that in the limit  $k\xi \gg 1$ , complete similarity indicates that the characteristic length becomes  $l \sim \xi$ , for both, spikes and bubbles. That is, a transition between this value and the one given by Eq. (11) must occur at some moment. The consequences of this will be discussed later.

In order to shed more light on the meaning of these characteristic lengths let us consider an idealized bubble in 2D geometry consisting in a long semicylinder of radius  $\xi_b$  (Fig. 2). In this manner we estimate the volume  $V_{b2}$  of the denser fluid (per unit length) that is displaced by the motion of the bubble, as  $V_{b2} \sim \pi \xi_b^2$ . Since the area of the interface per unit length is  $A_{b2} \sim \lambda$ , we have that the characteristic length that sets up the mass put in motion by the bubble in the nonlinear regime must be  $l_{2b}^{NL} \sim k \xi_b^2$ .

In the case of the spike, instead, the volume  $V_{s2}$  of the denser fluid being displaced would be  $V_{s2} \sim \xi_s \lambda$ , and since the area is  $A_{s2} \sim \lambda$ , we have that the mass of the denser fluid is mainly displaced vertically, in such a manner that it affects the mass within a distance of the order of  $l_{2s}^{NL} \sim \xi_s$ .

It is interesting to notice that during the nonlinear phase in which the bubble amplitude is still  $\xi_b < \lambda$ , mass conservation requires that  $V_{b2} \sim V_{s2}$  and, therefore, it is  $k \xi_b^2 \sim \xi_s$ . That is, if the spike is moving in free fall ( $\xi_s \sim t^2$ ), then it turns out  $\xi_b \sim t$ , and the bubble velocity must saturate. Besides, we also notice that the lateral motion of the bubble can only takes place while  $\xi_b < \lambda$ , and later it can only move vertically affecting the mass within a distance of the order of  $\xi_b$  from the interface. Therefore, the previously mentioned transition

in the motion has to occur when  $\xi_b \sim \lambda$  and, after, spike and bubble have to move in similar manner with  $l_{s,b} \sim \xi_{s,b}$ .

With these elements we can now extend the linear model to the nonlinear regime.

### C. Linear and nonlinear evolution

Let us first to consider the particular case of  $A_T = 1$ . Then the masses (per unit area) displaced by the spike and bubble, respectively, in the nonlinear regime (and for  $\xi_b < \lambda$ ) are as follows:

$$m_s^{\text{NL}} = \rho_2 l_{s2}^{\text{NL}} = C_1 \rho_2 \xi_s. \quad (12)$$

$$m_b^{\text{NL}} = \rho_2 l_{b2}^{\text{NL}} = C_2 \rho_2 k \xi_b^2. \quad (13)$$

Since in the linear regime these characteristic lengths are  $l_{s2}^L = l_{b2}^L = k^{-1}$ , we can describe both regimes together by interpolating the two characteristic lengths. For more accuracy in the transition region, but still keeping a relatively simple expression, we adopt a quadratic interpolation for the spike:

$$l_{s2} = \frac{1}{k} \sqrt{1 + (C_1 k \xi_s)^2}, \quad (14)$$

while for the bubble a linear interpolation is seen to be sufficient:

$$l_{b2} = \frac{1}{k} [1 + C_2 (k \xi_b)^2]. \quad (15)$$

When the light medium is also present ( $A_T < 1$ ), we can similarly consider that, in the bubble, the mass of light fluid will mainly move vertically displacing the mass within the characteristic length:

$$l_{b1} = \frac{1}{k} \sqrt{1 + (C_1 k \xi_b)^2}, \quad (16)$$

while, in the spike, the light fluid moves also laterally squeezing it, so that the characteristic length accounting for the displaced mass is as follows:

$$l_{s1} = \frac{1}{k} [1 + C_2 (k \xi_s)^2]. \quad (17)$$

Then the total mass (per unit area) that participates in the motion of the spike turns out:

$$m_s = \frac{\rho_1}{k} [1 + C_2 (k \xi_s)^2] + \frac{\rho_2}{k} \sqrt{1 + (C_1 k \xi_s)^2}, \quad (18)$$

and the equation of motion in Eq. (4) is as follows:

$$\frac{d}{dt} \left\{ \left[ \frac{\rho_1}{k} [1 + C_2 (k \xi_s)^2] + \frac{\rho_2}{k} \sqrt{1 + (C_1 k \xi_s)^2} \right] \dot{\xi}_s \right\} = (\rho_2 - \rho_1) g(t) \xi_s. \quad (19)$$

In the same manner, the total mass (per unit area) participating in the motion of the bubble, reads:

$$m_b = \frac{\rho_2}{k} [1 + C_2 (k \xi_b)^2] + \frac{\rho_1}{k} \sqrt{1 + (C_1 k \xi_b)^2}, \quad (20)$$

and the equation of motion for the bubble turns out:

$$\frac{d}{dt} \left\{ \left[ \frac{\rho_2}{k} [1 + C_2 (k \xi_b)^2] + \frac{\rho_1}{k} \sqrt{1 + (C_1 k \xi_b)^2} \right] \dot{\xi}_b \right\} = (\rho_2 - \rho_1) g(t) \xi_b. \quad (21)$$

As it can be seen, Eqs. (19) and (21) for  $\xi_s$  and  $\xi_b$ , respectively, become the same if  $\rho_1$  and  $\rho_2$  are interchanged and  $g$  is changed by  $-g$ . A property shared with Eqs. (1) and (2) for the BDM. However, the present equations do not include any drag force, consistently with the assumption of ideal fluids. Instead, it involves variable masses when the system enters in the nonlinear regime. Of course, a viscous drag term could also be incorporated to consider situations with finite Reynolds Re, provided that the function  $C_d = C_d(\text{Re})$  is known. But, certainly, it is not necessary when only inviscid fluids are considered.

As we have already mentioned, the lateral motion of the bubble cannot persist indefinitely and it must cease or strongly slow down at a time  $t = t_r$  when the bubble amplitude is  $\xi_b \sim \lambda$ . After this moment, the bubble motion will only displace mass in the vertical direction, and the characteristic length  $l_{b2}^{\text{NL}}$  will scale with the bubble amplitude  $\xi_b$ . At the same time  $l_{s1}^{\text{NL}}$  will scale with  $\xi_s$  and a transition (reacceleration) in the instability dynamics has to take place. For this, Eqs. (19) and (21) must be modified for  $t > t_r$  when  $\xi_b(t_r) \approx \lambda$ . We will come back on this point after analyzing the results of Eqs. (19) and (21).

For the analysis, we ignore for now the above mentioned transition for  $t > t_r$ . Moreover, we consider the particular case of constant gravity acceleration  $g$ . Then, we will write these equations in dimensionless form by defining the following dimensionless magnitudes:

$$z_{s,b} = k \xi_{s,b}; \quad T = t \sqrt{kg}. \quad (22)$$

Then, the evolution equations for the spike and bubble amplitudes, respectively read:

$$\frac{d}{dT} \left\{ [(1 - A_T)(1 + C_2 z_s^2) + (1 + A_T) \sqrt{1 + (C_1 z_s)^2}] \dot{z}_s \right\} = 2A_T z_s, \quad (23)$$

$$\frac{d}{dT} \left\{ [(1 + A_T)(1 + C_2 z_b^2) + (1 - A_T) \sqrt{1 + (C_1 z_b)^2}] \dot{z}_b \right\} = 2A_T z_b. \quad (24)$$

First integrals can be easily obtained:

$$\begin{aligned} & [(1 - A_T)(1 + C_2 z_s^2) + (1 + A_T) \sqrt{1 + (C_1 z_s)^2}]^2 \dot{z}_s^2 \\ &= 4A_T \left\{ (1 - A_T) \left[ \frac{z_s^2 - z_0^2}{2} + C_2 \frac{z_s^4 - z_0^4}{4} \right] \right. \\ & \quad \left. + \frac{(1 + A_T)}{3C_1^2} [1 + (C_1 z_s)^2]^{3/2} - [1 + (C_1 z_0)^2]^{3/2} \right\}, \end{aligned} \quad (25)$$

$$\begin{aligned} & [(1 + A_T)(1 + C_2 z_b^2) + (1 - A_T) \sqrt{1 + (C_1 z_b)^2}]^2 \dot{z}_b^2 \\ &= 4A_T \left\{ (1 + A_T) \left[ \frac{z_b^2 - z_0^2}{2} + C_2 \frac{z_b^4 - z_0^4}{4} \right] \right. \\ & \quad \left. + \frac{(1 - A_T)}{3C_1^2} [1 + (C_1 z_b)^2]^{3/2} - [1 + (C_1 z_0)^2]^{3/2} \right\}, \end{aligned} \quad (26)$$

where  $z_0 = z_s(t=0) = z_b(t=0)$  is the dimensionless initial amplitude, and we have put as initial conditions that  $\dot{z}_s(t=0) = \dot{z}_b(t=0) = 0$ .

#### D. Asymptotic behavior of spike and bubble

In the nonlinear regime it is  $z_{s,b} \gg 1$  and (ignoring reacceleration transition) Eqs. (23) and (24) turns out:

$$\frac{d}{dT} \left\{ [(1 - A_T)C_2 z_s^2 + (1 + A_T)C_1 z_s] \dot{z}_s \right\} = 2A_T z_s, \quad (27)$$

$$\frac{d}{dT} \left\{ [(1 + A_T)C_2 z_b^2 + (1 - A_T)C_1 z_b] \dot{z}_b \right\} = 2A_T z_b. \quad (28)$$

These equations can be integrated analytically to yield for the spike:

$$\begin{aligned} \frac{T}{2} = & \sqrt{\frac{1 - A_T}{4A_T} C_2 z_s^2 + \frac{1 + A_T}{3A_T} C_1 z_s} - \frac{(1 + A_T)C_1}{3\sqrt{A_T(1 - A_T)}C_2} \\ & \times \ln \left[ \frac{\sqrt{\frac{1 - A_T}{4} C_2 z_s + \frac{1 + A_T}{3} C_1} - \sqrt{\frac{1 - A_T}{4} C_2 z_s}}{\sqrt{\frac{1 + A_T}{3} C_1}} \right], \quad (29) \end{aligned}$$

and, for the bubble:

$$\begin{aligned} \frac{T}{2} = & \sqrt{\frac{1 + A_T}{4A_T} C_2 z_b^2 + \frac{1 - A_T}{3A_T} C_1 z_b} - \frac{(1 - A_T)C_1}{3\sqrt{A_T(1 + A_T)}C_2} \\ & \times \ln \left[ \frac{\sqrt{\frac{1 + A_T}{4} C_2 z_b + \frac{1 - A_T}{3} C_1} - \sqrt{\frac{1 + A_T}{4} C_2 z_b}}{\sqrt{\frac{1 - A_T}{3} C_1}} \right]. \quad (30) \end{aligned}$$

In order to take the limit for  $z_s \gg 1$  in Eq. (29) we must pay attention to the value of the Atwood number  $A_T$ . For  $(1 - A_T)z_s \gg 1$ , which excludes values of  $A_T$  too close to 1, we get:

$$z_s = \sqrt{\frac{A_T}{C_2(1 - A_T)}} T, \quad (31)$$

which agrees with the results of the potential theory by Goncharov [34] if we take  $C_2 = 3/2$ . In the opposite case of  $A_T$  sufficiently close to one, it will be  $(1 - A_T)z_s \ll 1$  even for large values of  $z_s$ . Then, we get:

$$z_s = \frac{A_T}{3C_1(1 + A_T)} T^2, \quad (32)$$

which returns the results for a free fall motion if we take  $C_1 = 1/3$ . Then, hereafter, we will take these values for  $C_1$  and  $C_2$ .

In a similar manner, by taking the limit  $z_b \gg 1$  in Eq. (30), it yields the following result for arbitrary  $A_T$ :

$$z_b = \sqrt{\frac{A_T}{C_2(1 + A_T)}} T, \quad (33)$$

which, again with  $C_2 = 3/2$ , agrees with the results of Refs. [34,35].

#### E. Comparison with the BDM

It is relevant to compare the results of the present model (PM) with those provided by the BDM such as given by Eqs. (1) and (2), since, although the issues discussed in

the Introduction, the BDM it is known to yield a correct outcome because it has been constructed to fit the results of experiments and numerical simulations and, therefore, it can be considered as a good compilation of such results. For this we have solved the ordinary differential equations for the BDM [Eqs. (1) and (2)], and for the PM [Eqs. (25) and (26)], respectively, by means of the commercial software MATHEMATICA Computer Code [46].

In Fig. 3 we show the outputs of the present model together with those of the BDM for the spike and bubble amplitudes, for three values of the Atwood number:  $A_T = 1, 0.5$ , and  $0.1$  and for three values of the dimensionless initial amplitude:  $z_0 = 0.01, 0.1$ , and  $1$ . The present model produces essentially the same results as the BDM.

To better quantify the differences we have plotted in Fig. 4 the ratio of the amplitudes given by the PM and the BDM for  $A_T = 1$  and  $A_T = 0.1$ . The case for  $A_T = 1$ , in Fig. 4(a), is the one presenting the largest difference for the largest initial amplitude  $z_0 = 1$ . Nevertheless, it is always less than 18% and it occurs for the intermediate times due the different procedures for matching the linear and the nonlinear regimes adopted in each model. The difference reduces to less than 8% for  $A_T = 0.1$  in Fig. 4(b), and once again, it happens for the intermediate times but, in this case, for the smallest amplitude.

In Fig. 5 we have represented the spike and bubble velocity evolutions corresponding to the amplitudes shown in Fig. 3.

The present model shows that the saturation of the bubble velocity for any  $A_T$  occurs as a consequence of the prevalence of the denser fluid mass displaced laterally during the bubble evolution, which increases with time. And for  $A_T < 1$ , the spike velocity also saturates because the lateral displacement of the light fluid gets the control of the dynamics. Of course, the lighter fluid is absent for  $A_T = 1$  and, therefore, the spike velocity does not saturate.

However, as we have previously mentioned, the lateral displacement of the denser fluid due to the bubble motion, cannot persist after the bubble have achieved an amplitude  $\xi_b$  of the order of  $\lambda$ . In fact, the widening of the bubble implies the narrowing of the spike and so, mass conservation imposes that spike amplitude tends to infinity when the bubble wide tends to  $\lambda$  [47]. Such a condition must also limit the potential models like the one in Ref. [34]. This limitation is also very evident in the theory by Ott [48] for the nonlinear RTI in a thin layer. Therefore, for  $\xi_b > \lambda$ , mass displacement by the bubble and by the spike can only happens in the vertical direction affecting the mass within a characteristic distance  $l_{s,b} \sim \xi_{s,b}$ , for the spike and the bubble, respectively. A schematic picture of the evolution of the characteristic length for the bubble is shown in Fig. 6.

Then, under the present physical picture, Eqs. (19) and (21) cannot be used after the time  $t_r$  when  $\xi_b(t_r) \approx \lambda$ . In this manner a natural explanation for the reacceleration process arises that is independent of the vorticity generation by the accompanying KHI, which indeed, must be absent for  $A_T = 1$  when reacceleration should still occur, such as it has been inferred from recent numerical simulations [37], provided that the fluid is inviscid (infinite Reynolds number). Instead, reacceleration is shown here to be a consequence of the reduction of mass involved in the motion during the instability evolution for  $t > t_r$ .

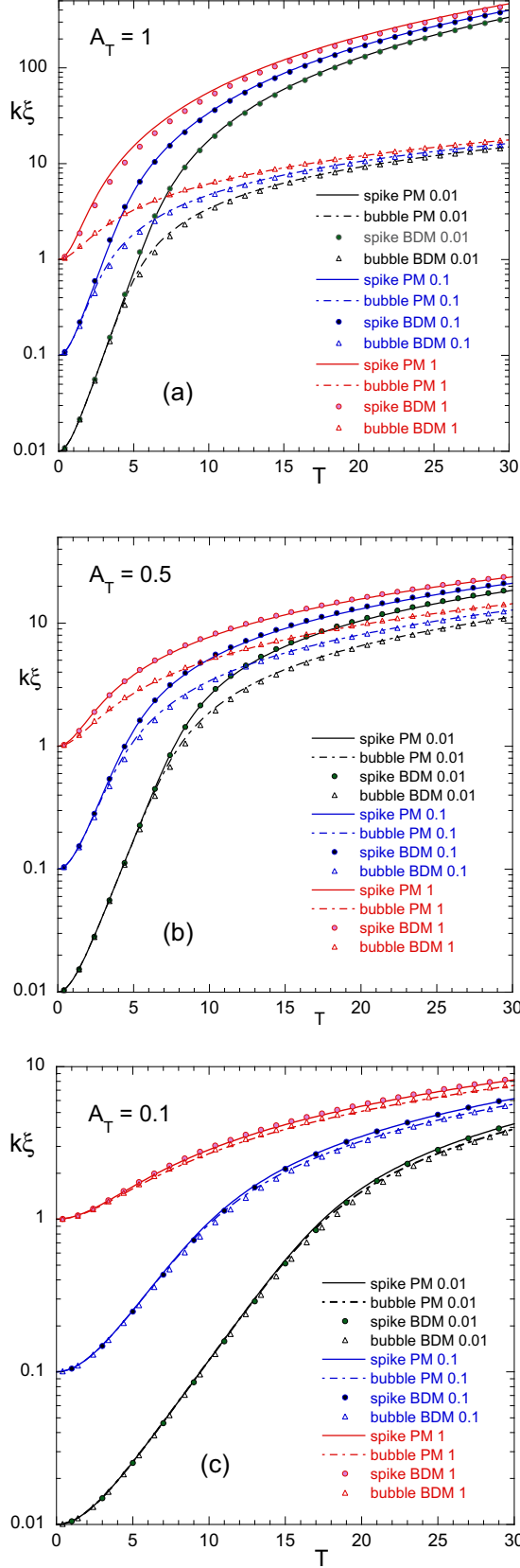


FIG. 3. Spike and bubble amplitude evolutions. Comparison of the present model (PM) with the BDM for three dimensionless initial amplitudes:  $z_0 = 0.01$  (black),  $z_0 = 0.1$  (blue), and  $z_0 = 1$  (red); and for three values of the Atwood numbers: (a)  $A_T = 1$ , (b)  $A_T = 0.5$ , and (c)  $A_T = 0.1$ .

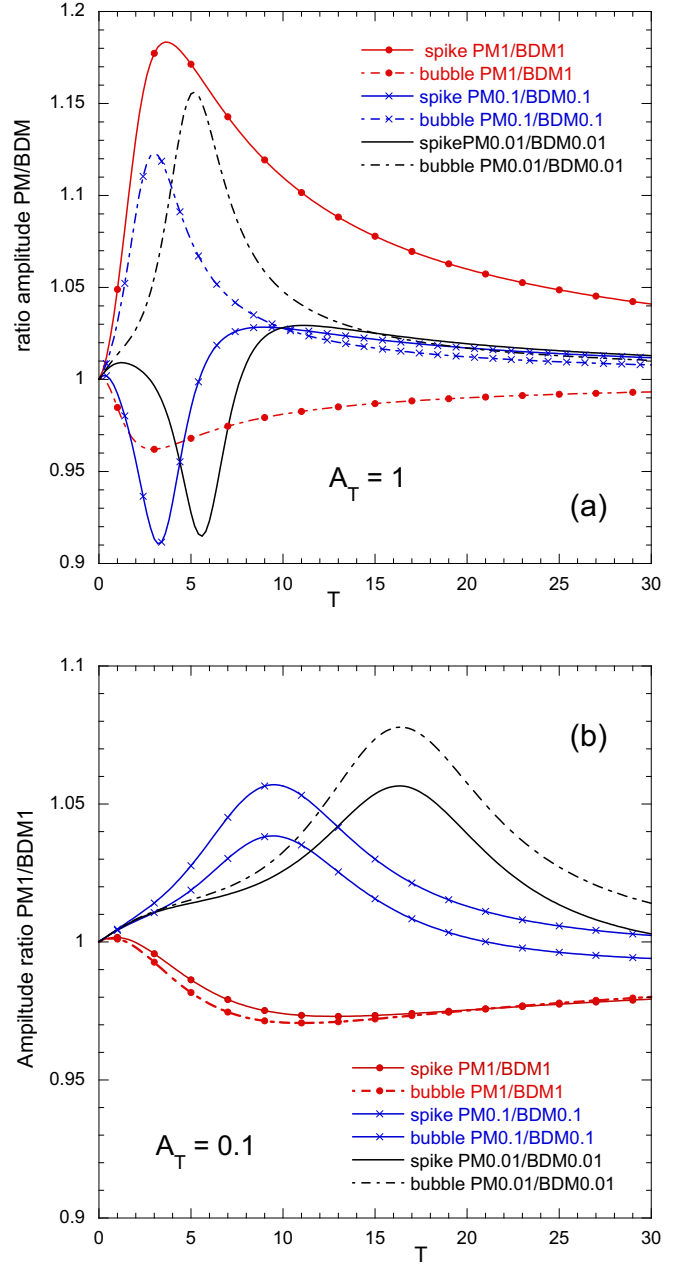


FIG. 4. Amplitude ratio between the present model (PM) with the BDM for three dimensionless initial amplitudes:  $z_0 = 0.01$  (black-smooth lines),  $z_0 = 0.1$  (blue-cross lines), and  $z_0 = 1$  (red-circle lines); and for three values of the Atwood numbers: (a)  $A_T = 1$  and (b)  $A_T = 0.1$ .

### III. SPIKE AND BUBBLE REACCELERATION

When  $t = t_r$  the bubble amplitude is  $\xi_b \approx \lambda$ , the new added mass of denser fluid  $m_{b2}$  participating in the bubble motion scales like  $2\pi C_2 \xi_b \rho_2$ , and the mass of lighter fluid  $m_{s1}$  corresponding to the spike motion scales like  $C_1 \xi_s \rho_1$ . The added masses of light and dense fluids that are put in motion by the bubble and the spike, respectively, remain without change because they cannot be further reduced. Then, since it occurs in the nonlinear phase, we neglect the initial linear phase, and

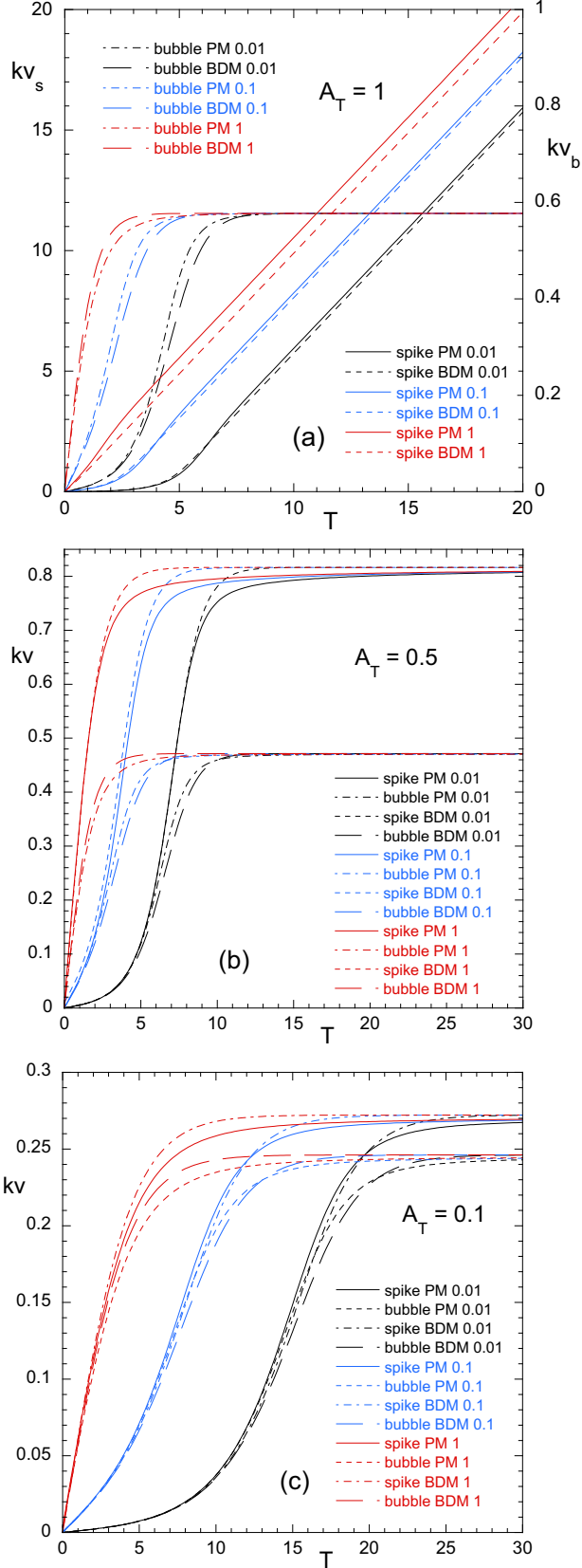


FIG. 5. Spike and bubble velocity evolutions. Comparison of the present model (PM) with the BDM for three dimensionless initial amplitudes:  $z_0 = 0.01$  (black bottom curves),  $z_0 = 0.1$  (blue middle curves), and  $z_0 = 1$  (red top curves); and for three values of the Atwood numbers: (a)  $A_T = 1$ , (b)  $A_T = 0.5$ , and (c)  $A_T = 0.1$ .

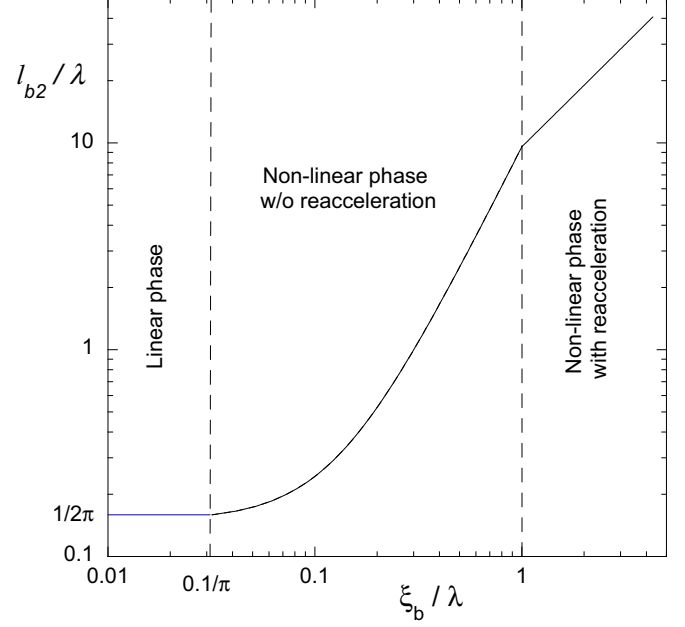


FIG. 6. Schematic of the characteristic length  $l_{b2}$ , determining the mass participating in the motion of the bubble, as a function of the bubble perturbation amplitude  $\xi_b / \lambda$ .

the total masses turns out:

$$m_s = (2\pi C_2 \rho_1 + C_1 \rho_2) \xi_s; \quad m_b = (2\pi C_2 \rho_2 + C_1 \rho_1) \xi_b. \quad (34)$$

Then the resulting equations of motion in dimensionless form, and for  $T > T_r$  [ $z_b(T_r) = z_{br} = 2\pi$  and  $z_s(T_r) = z_{sr}$ ], are as follows:

$$\frac{d}{dT} (C_{s3} z_s \dot{z}_s) = A_T z_s, \quad (35)$$

$$\frac{d}{dT} (C_{b3} z_b \dot{z}_b) = A_T z_b, \quad (36)$$

where

$$C_{s3} = \frac{1 + A_T}{2} C_1 + 2\pi \frac{1 - A_T}{2} C_2, \quad (37)$$

$$C_{b3} = \frac{1 - A_T}{2} C_1 + 2\pi \frac{1 + A_T}{2} C_2. \quad (38)$$

These equations admit a first integral:

$$z_s \dot{z}_s = \sqrt{\frac{2A_T}{3C_{s3}} (z_s^3 - z_{sr}^3) + z_{sr}^2 \dot{z}_{sr}^2}, \quad (39)$$

$$z_b \dot{z}_b = \sqrt{\frac{2A_T}{3C_{b3}} (z_b^3 - z_{br}^3) + z_{br}^2 \dot{z}_{br}^2}, \quad (40)$$

where  $\dot{z}_{sr} = \dot{z}_s(T_r)$  and  $\dot{z}_{br} = \dot{z}_b(T_r)$ . Asymptotically,  $z_{s,b} \gg z_{sr,br}$ , and we get:

$$z_s \approx \frac{A_T}{6C_{s3}} T^2; \quad z_b \approx \frac{A_T}{6C_{b3}} T^2. \quad (41)$$

In particular, for  $A_T = 1$ , it is  $C_{s3} = C_1 = 1/3$  and  $C_{b3} = 2\pi C_2 = 3\pi$  and both, spike and bubble velocities, grow linearly with time (for  $T > T_r$ ). The dynamics of the spike is not changed in this case and it grows asymptotically at the

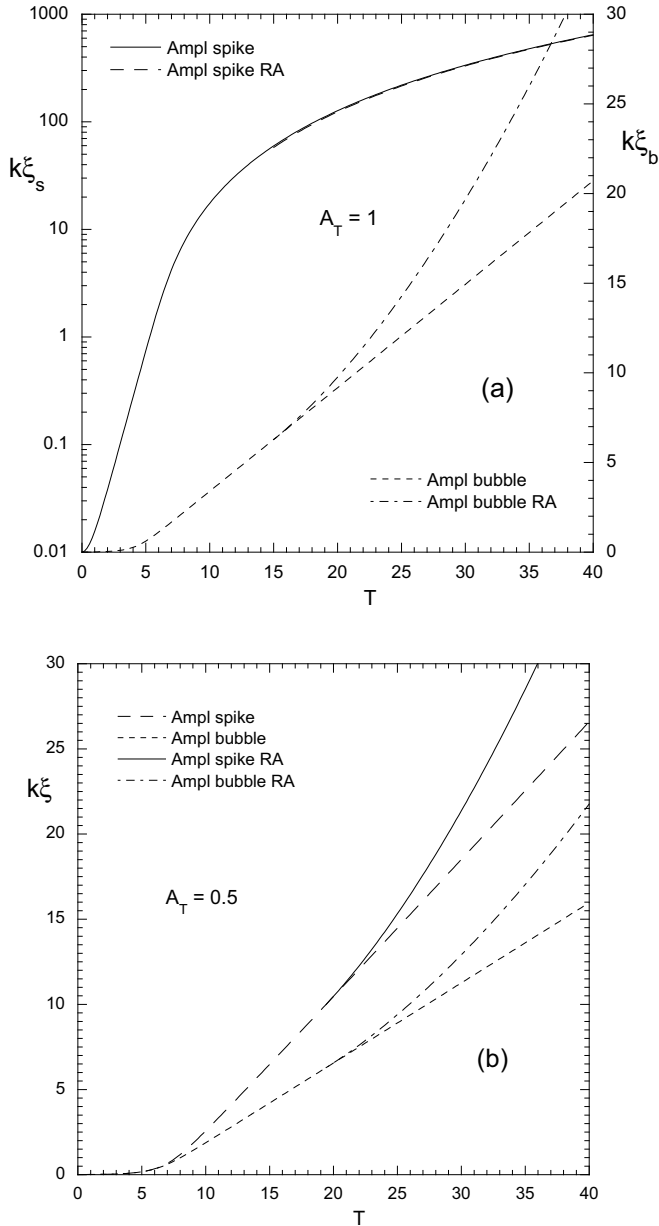


FIG. 7. Spike and bubble amplitudes with and without reacceleration. (a)  $A_T = 1$ , (b)  $A_T = 0.5$ .

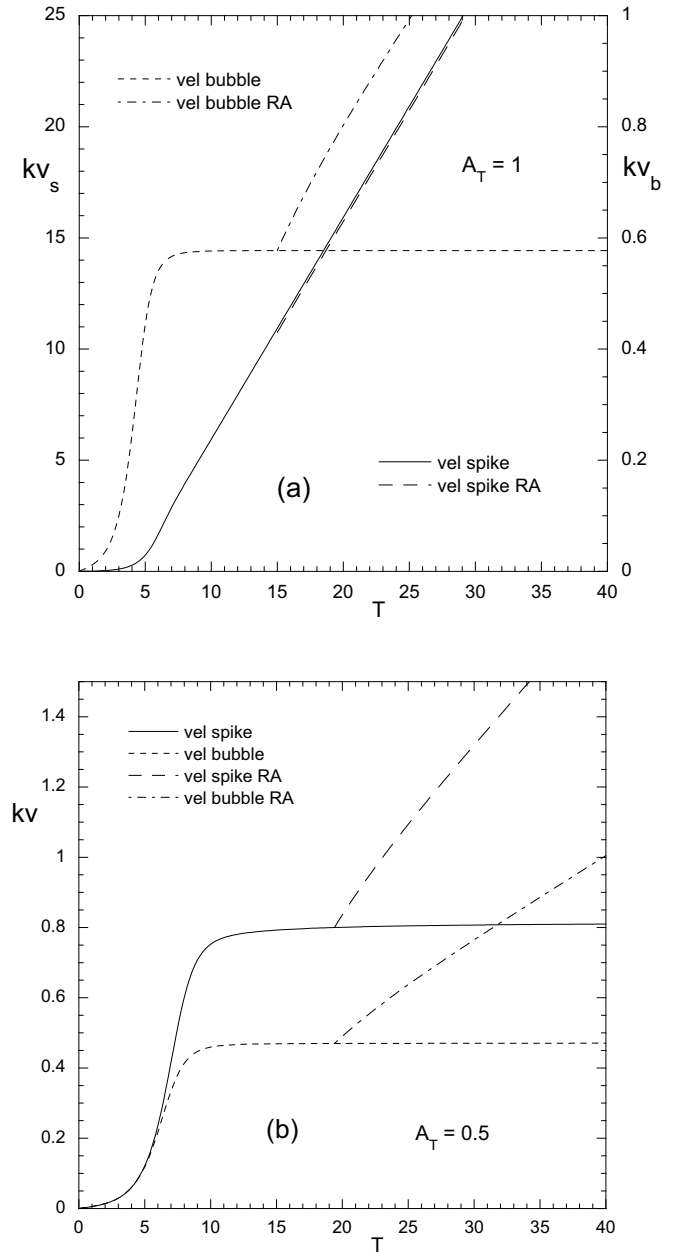


FIG. 8. Spike and bubble velocities with and without reacceleration. (a)  $A_T = 1$ , (b)  $A_T = 0.5$ .

same rate as with no bubble reacceleration. But the bubble, which had achieved a constant velocity at  $T = T_r$  (saturation), is reaccelerated at later times.

For  $A_T < 1$ , when the spike velocity also saturates, it is also reaccelerated at  $T = T_r$  but with an acceleration, in general, different than that of the bubble. For  $A_T \ll 1$ , it becomes  $C_{s3} \approx C_{b3}$  and spikes and bubbles are reaccelerated at the same rate.

In Fig. 7 we have represented the spike and bubble amplitude evolutions for two values of  $A_T$  with and without reacceleration. For  $A_T = 1$  in Fig. 7(a), spike evolution is not modified but the bubble velocity increases at  $T = T_r$ . And for  $A_T = 0.5$ , in Fig. 7(b) both are reaccelerated. Figure 8 shows the corresponding velocities.

We want to remark that in the present physical picture, reacceleration appears as a consequence of the transition undergone by the bubble dynamics when  $\xi_b \approx \lambda$  and it has to stop or strongly slow down its lateral motion. This is a process independent of the vorticity generated by the KHI which necessarily happens only for  $A_T < 1$ , and is consistent with the observation by Wilkinson and Jacob [39] about the absence of reacceleration in the Waddell *et al.* [43] experiments for low Atwood numbers, although the evident presence of vortices created by the shear produced by the spike penetration into the lighter fluid. Such results are in agreement with the longer time required for the bubble to achieve an amplitude  $\xi_b \approx \lambda$ , which could also have undergone an extra delay by the presence of viscosity [37,49].



#### IV. TWO-DIMENSIONAL NUMERICAL SIMULATIONS FOR $A_T = 1$

In order to compare with the results of the present model, we have performed a series of 2D numerical simulations with the explicit version of the finite-element code ABAQUS [50].

For this, following Ref. [51] we have considered a plate of thickness  $h = 4\lambda$  so that it would behave as an infinite plate at least until the bubble amplitude achieves a value  $\xi_b \sim 2\lambda$ . Then, the plate was meshed with  $40 \times 160$  2D continuum four node bilinear elements with reduced integration and hour-glassing control.

We consider an aluminium plate of density  $\rho = 2700$  kg/m<sup>3</sup> in a uniform and constant gravitational field  $g = 10^7$  m/s<sup>2</sup>. The plate material does not have constitutive properties so that it is treated as an ideal medium (the deviatoric part of the stress tensor is equal to zero). For the equation of state, the Mie-Grüneisen equation has been adopted with a Grüneisen coefficient  $\Gamma = \rho_0 \Gamma_0 / \rho$  ( $\Gamma_0$  is a material parameter). For expressing the Hugoniot of the medium, we have taken the usual linear relationship between the shock velocity  $v_s$  and the particle velocity  $v_p$ :

$$v_s = c'_0 + s v_p, \quad (42)$$

$$p - p_h = \rho_0 \Gamma_0 (\epsilon - \epsilon_h), \quad (43)$$

where “ $h$ ” denotes the Hugoniot reference state and  $\epsilon$  is the specific internal energy. The constants  $c'_0$  and  $s$  are characteristic parameters of the material. For the present case in which the medium is aluminum we have  $\Gamma_0 = 2.16$ ,  $s = 1.337$ . In order to assure incompressible perturbations ( $\delta\rho/\rho \ll 1$ ) we require that  $c'_0 \sim c_s \gg \sqrt{g/k}$  and, for this, we have taken  $c'_0 \sim 10c_0$  ( $c_0 = 5380$  m/s is the sound speed).

There is a uniform pressure  $p_0 = \rho g h$  at the bottom of the plate and the instability is seeded with an initial sinusoidal perturbation  $\xi_0 \sin kx$  applied at such a surface, and its amplitude decreases linearly toward top of the plate.

In Fig. 9 we show the results for the spike and bubble amplitude evolutions for two different initial amplitudes and their corresponding wavelengths in order to have  $k\xi_0 = 0.01$  and  $k\xi_0 = 0.5$  in Figs. 8(a) and 8(b), respectively. To prevent the premature calculation termination as a result of severe mesh distortion, an arbitrary Lagrangian-Eulerian adaptive meshing technique has been applied to the bubble zone, remaining the spike zone under a Lagrangian description to deform into the vacuum. Nevertheless, calculation stops when  $\xi_b \sim \lambda$  and the mesh in the spikes becomes too distorted, making the region  $\xi_b > \lambda$  inaccessible to our numerical calculations. As a consequence, bubble reacceleration cannot be observed. However, for  $\xi_b \leq \lambda$  model and simulations are in excellent agreement.

In Fig. 10 we have represented the spike and bubble velocities as a function of time for the same cases as in Fig. 9. They turns out to be somewhat noisy but, in average the simulations results agree with the theoretical model.

Unfortunately, ABAQUS code seems to be not suitable for following the spike and bubble evolutions at longer times. In addition, it is neither appropriate for situations with  $A_T < 1$  in which the KHI is present, thus submitting the mesh to strong deformations that force to stop the calculation at rather early

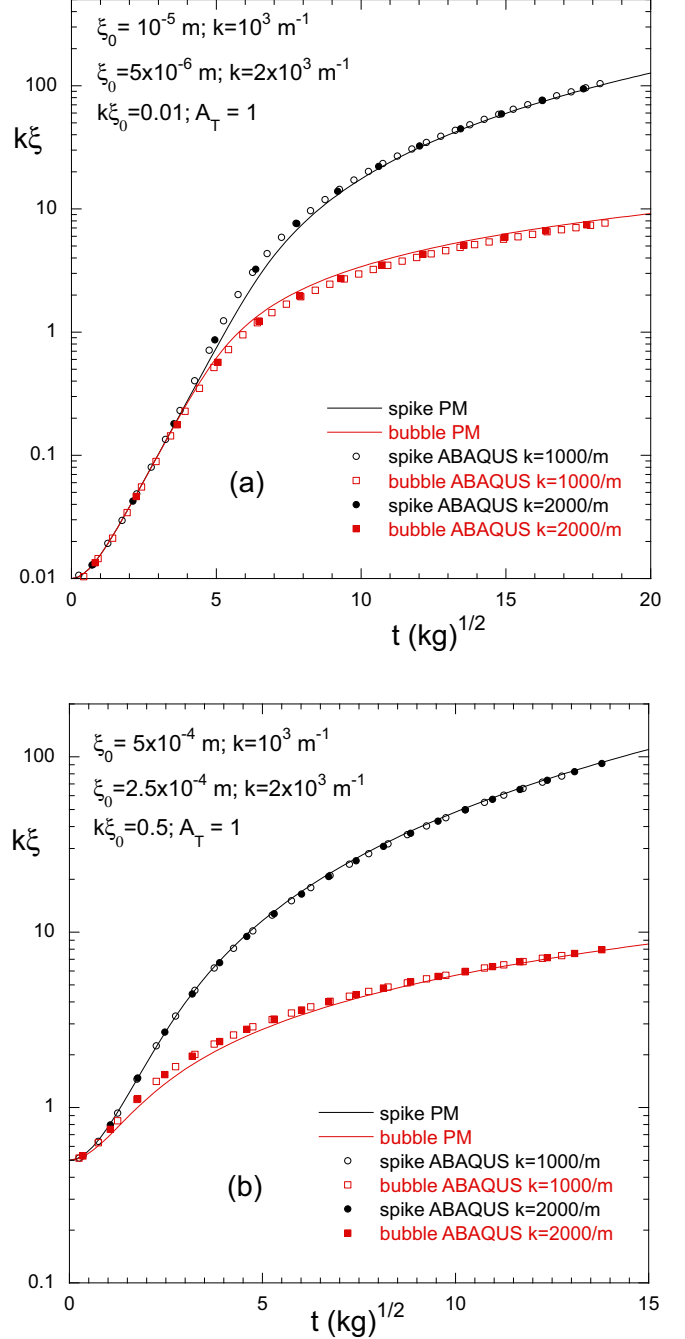


FIG. 9. Spike and bubble amplitudes evolution for  $A_T = 1$  given by the present model (full lines) and 2D numerical simulations (dots) for (a)  $k\xi_0 = 0.01$  and (b)  $k\xi_0 = 0.5$ .

times in the nonlinear regime. Therefore, a direct numerical simulation study to observe the bubble reacceleration for  $A_T = 1$ , such as it has been inferred in Ref. [37], and it is also suggested by the present theory, remains still missing.

#### V. DISCUSSION AND CONCLUDING REMARKS

We have constructed an analytical model based on the Newton’s second law, for the single mode, 2D RTI in inviscid, incompressible and immiscible ideal fluids, that extends a previous linear theory for the linear regime. To this end, we have

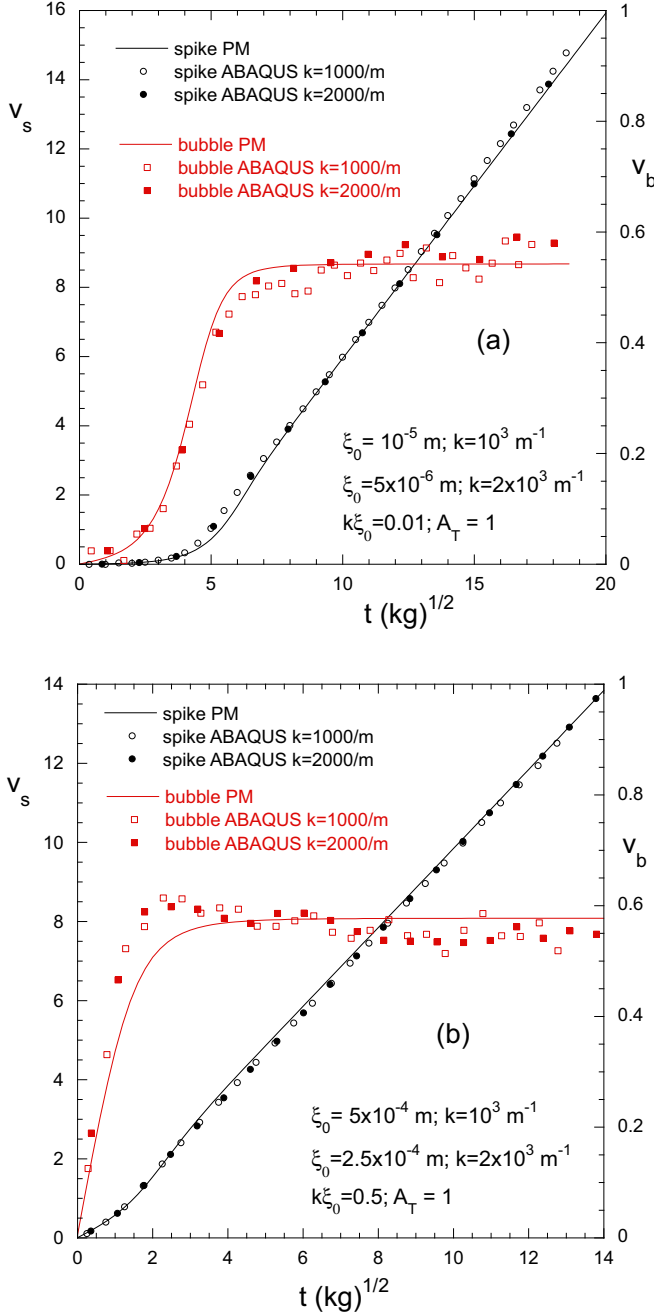


FIG. 10. Spike and bubble velocities evolution for  $A_T = 1$  given by the present model (full lines) and 2D numerical simulations (dots) for (a)  $k\xi_0 = 0.01$  and (b)  $k\xi_0 = 0.5$ .

considered on the basis of dimensional analysis and physical arguments that, in the nonlinear regime, the masses of both fluids involved in the motion during the amplitude growth, changes as the perturbation evolves.

This consideration includes the mass displaced laterally while the bubble widens and the spike narrows in the earliest stage of the nonlinear regime. Such a feature leads to the saturation of the bubble velocity for any value of the Atwood number  $A_T$ , and also to the spike velocity saturation for  $A_T < 1$  while the dynamics is controlled by such laterally displaced mass. Thus, velocity saturation occurs without the

necessity to introduce any drag force which, on the other hand, is inconsistent with the inviscid fluids assumption. However, this early stage cannot persist for a long time, since the lateral dimension of the spike plus the bubble, included the mass it displaces, is limited to the size of a wavelength.

Therefore, for  $\xi_b > \lambda$  there is a second phase of growth dominated by the vertical displacement of the mass participating in the motion in which the new added mass is less in comparison with the previous phase, thus leading to the increase of the perturbation velocity. This reacceleration phase takes place independently of the vorticity generated by the onset of the KHI which, in any case, would be unable to accelerate the perturbation growth because it is the penetration of the spike into the lighter fluid what produces the shear causing the vortices. Not in other way around as it seems to suggest the KHI arguments about vortices powering the perturbation growth that is often given to explain reacceleration.

The physical picture we are presenting for the reacceleration process is consistent with its absence when the bubble amplitude  $\xi_b$  has not yet achieved a magnitude of the order of  $\lambda$  and yet, there is a clear presence of vortices generated by KHI [39,43]. An it is also consistent with the observation that bubble reacceleration must also occur for  $A_T = 1$  in inviscid media [37]. Nevertheless, KHI could perhaps be responsible for other effects observed in numerical simulations, like the velocity oscillations during the reacceleration phase, provided that such oscillations are not related to the necessary limitations in the computational domain, which may need to be considerably larger than the region affected by the instability. Such a region remains constant in the linear phase and of the order of  $k^{-1}$ , but in the nonlinear regime, it will grow with the perturbation amplitude.

Furthermore, it is improbable that the potential theories can describe the transition taking place when  $\xi_b \approx \lambda$  because they deal with the perturbations and conservation equations in the region near the tip of the bubble. Therefore, the limitation in the bubble lateral motion may not be captured. Such a limit, however, is clearly seen in the theories of Refs. [47,48].

The effects of the viscosity are not included in the present theory. It could probably be considered in a similar manner as it is done with the drag force in the BDM, provided that it is accepted that viscous drag in the present 2D problem can be in some way assimilated to the problem of a solid body penetrating into a fluid, or to the problem of a single rising bubble [52]. Even though, the general dependence of the drag coefficient  $C_d$  on the Reynolds number  $Re$  should be taken into account in order to reflect the behavior at the different velocities in the linear and the nonlinear regimes. Indications in this sense are found in Ref. [44] where for the linear regime, corresponding to the lowest velocities, the drag force  $F_d$  (per unit area) was found to be  $F_d = 2\mu k\dot{\xi}$ , and the drag coefficient is  $C_d = 2F_d/\rho\dot{\xi}^2 = 8\pi/Re$ , where  $Re = \rho\dot{\xi}\lambda/\mu$  and  $\mu$  is the dynamic viscosity.

Instead, for high Reynolds numbers,  $C_d$ , experiments with solid bodies and with single rising bubbles show that  $C_d$  becomes practically independent of  $Re$ . This result is also supported by dimensional analysis, since complete similarity yields  $C_d = \phi(Re)$  and, for  $Re \gg 1$ ,  $\phi(Re)$  must tend to a nonzero constant. Therefore, even at  $Re = 30000$  as considered in Ref. [37] it is still present a drag force that affects the

dynamics of the bubble. Such a behavior is known to persist for a wide range of  $Re$  ( $100 < Re < 10^5$ ) with little variation of the  $C_d$  value. As a consequence,  $Re > 10^5$ – $10^6$  may be necessary to observe the fluid behaving as inviscid, thus requiring very high resolutions in the numerical simulations in order to achieve the inviscid fluid regime.

On the other hand, different to the BDM case, an extension to 3D may require something else than a change in the values of the fitting constants. In fact, the present theory suggests a different scaling for the characteristic length that determines the mass involved in its motion in the regime  $\xi_b < \lambda$ .

Besides, it is noticed that the theory can be applied to arbitrary time evolutions of the gravity acceleration. In particular, it can be easily used for the case of an impulsive acceleration in order to model the Richtmyer-Meshkov instability.

Finally, it may be worth to mention that the present physical picture is also consistent with the absence of saturation in the bubble velocity in solid media observed in Ref. [51], in which the elastic-plastic lateral forces prevent the bubble formation, thus considerably extending the phase of exponential growth until the perturbation wavelength amplitude stops being the only relevant characteristic length.

#### ACKNOWLEDGMENTS

This work has been partially supported by MICIU/AEI/10.13039/501100011033 and FEDER, EU (Grant No. PID2021-125550OB-I00), the UCLM (Grant No. 2022-GRIN-34299), and by the BMBF of Germany. Discussions with M. Temporal are acknowledged.

- 
- [1] Y. Zhou, *Phys. Rep.* **720-722**, 1 (2017).  
 [2] Y. Zhou, *Phys. Rep.* **723-725**, 1 (2017).  
 [3] H. J. Kull, *Phys. Rep.* **206**, 197 (1991).  
 [4] O. Blaes, R. Blandford, and P. Madau, *Astrophys. J.* **363**, 612 (1990).  
 [5] G. H. Houseman and P. Molnar, *Geophys. J. Int.* **128**, 125 (1997).  
 [6] A. Burrows, *Nature (London)* **403**, 727 (2000).  
 [7] E. B. Burov and P. Molnar, *Earth Planet. Sci. Lett.* **275**, 370 (2008).  
 [8] A. R. Piriz, S. A. Piriz, and N. A. Tahir, *Phys. Rev. E* **100**, 063104 (2019).  
 [9] S. A. Piriz, A. R. Piriz, N. A. Tahir, S. Richter, and M. Bestehorn, *Phys. Rev. E* **103**, 023105 (2021).  
 [10] A. R. Piriz, S. A. Piriz, and N. A. Tahir, *Phys. Rev. E* **104**, 035102 (2021).  
 [11] A. R. Piriz, S. A. Piriz, and N. A. Tahir, *Phys. Rev. E* **106**, 015109 (2022).  
 [12] A. R. Piriz, S. A. Piriz, and N. A. Tahir, *Phys. Rev. E* **107**, 035105 (2023).  
 [13] J. F. Barnes, P. J. Blewett, R. G. McQueen, K. A. Meyer, and D. Venable, *J. Appl. Phys.* **45**, 727 (1974).  
 [14] N. A. Tahir, I. V. Lomonosov, B. Borm, A. R. Piriz, P. Neumayer, A. Shutov, V. Bagnoud, and S. A. Piriz, *Contrib. Plasma Phys.* **57**, 493 (2017).  
 [15] N. A. Tahir, A. Shutov, A. R. Piriz, P. Neumayer, I. V. Lomonosov, V. Bagnoud, and S. A. Piriz, *Contrib. Plasma Phys.* **59**, e201800135 (2019).  
 [16] N. A. Tahir, P. Neumayer, A. Shutov, A. R. Piriz, I. V. Lomonosov, V. Bagnoud, S. A. Piriz, and C. Deutsch, *Contrib. Plasma Phys.* **59**, e201800143 (2019).  
 [17] N. A. Tahir, P. Neumayer, I. V. Lomonosov, A. Shutov, V. Bagnoud, A. R. Piriz, S. A. Piriz, and C. Deutsch, *Phys. Rev. E* **101**, 023202 (2020).  
 [18] D. H. Kalantar, B. A. Remington, J. D. Colvin, K. O. Mikaelian, S. V. Weber, L. G. Wiley, J. S. Wark, A. Loveridge, A. M. Allen, A. A. Hauer, and M. A. Meyers, *Phys. Plasmas* **7**, 1999 (2000).  
 [19] J. D. Colvin, M. Legrand, B. A. Remington, G. Shurtz, and S. V. Weber, *J. Appl. Phys.* **93**, 5287 (2003).  
 [20] B. A. Remington, P. Allen, E. M. Bringa, J. Hawreliak, D. Ho, K. T. Lorenz, H. Lorenzana, J. M. McNaney, M. A. Meyers, S. W. Pollaine, K. Rosolankova, B. Sadik, M. S. Schneider, D. Swift, J. Wark, and B. Yaakobi, *Mater. Sci. Technol.* **22**, 474 (2006).  
 [21] D. M. Sterbentz, C. F. Jekel, D. A. White, and J. L. Belof, *Phys. Fluids* **34**, 082109 (2022).  
 [22] R. S. Craxton, K. S. Anderson, T. R. Boehly, V. N. Goncharov, D. R. Harding, J. P. Knauer, R. L. McCrory, P. W. McKenty, D. D. Meyerhofer, J. F. Myatt, A. J. Schmitt, J. D. Sethian, R. W. Short, S. Skupsky, W. Theobald, W. L. Kruer, K. Tanaka, R. Betti, T. J. B. Collins, J. A. Delettrez *et al.*, *Phys. Plasmas* **22**, 110501 (2015).  
 [23] O. A. Hurricane, P. K. Patel, R. Betti, D. H. Froula, S. P. Regan, S. A. Slutz, M. R. Gomez, and M. A. Sweeney, *Rev. Mod. Phys.* **95**, 025005 (2023).  
 [24] B. Bachmann, S. A. MacLaren, L. Masse, S. Bhandarkar, T. Briggs, D. Casey, L. Divol, T. Döppner, D. Fittinghoff, M. Freeman, S. Haan, G. N. Hall, B. Hammel, E. Hartouni, V. Geppert-Kleinrath, S. Khan, B. Koziolowski, C. Krauland, O. Landen, D. Mariscal *et al.*, *Phys. Plasmas* **30**, 052704 (2023).  
 [25] N. A. Tahir and K. A. Long, *Atomkernenergie-Kerntechnik* **40**, 157 (1982).  
 [26] N. A. Tahir and K. A. Long, *Phys. Lett. A* **90**, 242 (1982).  
 [27] J. C. V. Hansom, P. A. Rosen, T. J. Goldsack, K. Oades, P. Fieldhouse, N. Cowperthwaite, D. L. Youngs, N. Mawhinney, and A. J. Baxter, *Laser Part. Beams* **8**, 51 (1990).  
 [28] U. Alon, J. Hecht, D. Ofer, and D. Shvarts, *Phys. Rev. Lett.* **74**, 534 (1995).  
 [29] G. Dimonte, *Phys. Plasmas* **7**, 2255 (2000).  
 [30] B. Cheng, J. Glimm, and D. H. Sharp, *Phys. Lett. A* **268**, 366 (2000).  
 [31] Y. Srebro, Y. Elbaz, O. Sadot, L. Arazi, and D. Shvarts, *Laser Part. Beams* **21**, 347 (2003).  
 [32] D. Oron, L. Arazi, D. Kartoon, A. Rikanati, U. Alon, and D. Shvarts, *Phys. Plasmas* **8**, 2883 (2001).  
 [33] K. Balakrishnan and S. Menon, *Laser Part. Beams* **29**, 201 (2011).  
 [34] V. N. Goncharov, *Phys. Rev. Lett.* **88**, 134502 (2002).

- [35] J. Hecht and U. Alon, and D. Shvarts, *Phys. Fluids* **6**, 4019 (1994).
- [36] J. Xin, Y. Liu, X. Jiang, R. Yan, J. Li, Z.-H. Wan, D.-J. Sun, and J. Zheng, *Phys. Plasmas* **30**, 112702 (2023).
- [37] X. Bian, D. Zhao, H. Zhang, and D. Livescu, *Physica D* **403**, 132250 (2020).
- [38] P. Ramaprabhu, G. Dimonte, Y.-N. Young, A. C. Calder, and B. Fryxell, *Phys. Rev. E* **74**, 066308 (2006).
- [39] J. P. Wilkinson and J. W. Jacobs, *Phys. Fluids* **19**, 124102 (2007).
- [40] P. Ramaprabhu, G. Dimonte, P. Woodward, C. Fryer, G. Rockefeller, K. Muthuraman, P.-H. Lin, and J. Jayaraj, *Phys. Fluids* **24**, 074107 (2012).
- [41] R. Betti and J. Sanz, *Phys. Rev. Lett.* **97**, 205002 (2006).
- [42] N. R. Hanson, *Rev. Metaphys.* **19**, 133 (1965).
- [43] J. T. Waddell, C. E. Niederhaus, and J. W. Jacobs, *Phys. Fluids* **13**, 1263 (2001).
- [44] A. R. Piriz, O. D. Cortázar, J. J. López Cela, O. D. Cortázar, and N. A. Tahir, *Am. J. Phys.* **74**, 1095 (2006).
- [45] G. I. Barenblatt, *Scaling, Self-similarity, and Intermediate Asymptotics* (Cambridge University Press, New York, 1996).
- [46] MATHEMATICA Computer Code, version 13.2.10 (Wolfram Research, Inc., Champaign, IL, 2022).
- [47] J. K. Dienes, *Phys. Fluids* **21**, 736 (1978).
- [48] E. Ott, *Phys. Rev. Lett.* **29**, 1429 (1972).
- [49] Z.-X. Hu, Y.-S. Zhang, B. Tian, Z. He, and L. Li, *Phys. Fluids* **31**, 104108 (2019).
- [50] H. Hibbitt, B. Karlsson, and P. Sorensen, *Abaqus User Subroutine Reference Manual Version 6.10* (Dassault Systèmes Simulia Corp, USA, 2011).
- [51] A. R. Piriz, J. J. López Cela, S. A. Piriz, and N. A. Tahir, *Phys. Rev. E* **108**, 055102 (2023).
- [52] A. Tomiyama, I. Kataoka, I. Zun, and T. Sakaguchi, *JSME Int. J., Ser. B* **41**, 472 (1998).